Modeling and Simulation of Fiber Reinforced Polymer Mold Filling Process by Level Set Method

Binxin Yang[1]**, Jie Ouyang**[1]**, Tao Jiang**[1] **and Chuntai Liu**[2]

Abstract: A gas-solid-liquid three-phase model is proposed for fiber reinforced composites mold filling process. The fluid flow is described in Eulerian coordinate while the dynamics of fibers is described in Langrangian coordinate. The interaction of fluid flow and fibers are enclosed in the model. The influence of fluid flow on fibers is described by the resultant forces imposed on fibers and the influence of fibers on fluid flow is described by the momentum exchange source term in the model. A finite volume method coupled with a level set method for viscoelastic-Newtonian fluid flow is used to solve the model. The direct dynamic numerical simulation for reinforced composites mold filling process is realized. The information about fiber transformation and orientation and interface evolution are obtained dynamically as well as the information about pressure and velocity etc. The skin-core-skin structure of fibers under different slenderness ratios during the mold filling process is captured which is in accordance with experimental results.

Keywords: fiber reinforced composites, mold filling, finite volume method, viscoelastic, fiber orientation

1   Introduction

The plastic mold filling process produces large numbers of parts of high quality. Plastic material in the form of granules is melted until soft enough to be injected under pressure to fill a mold. Early simulations of mold filling process mostly used the Hele-Shaw model coupled with the finite element method, which is based on the creeping flow lubrication model [Wang, Hieber and Wang (1986); Chiang Hieber and Wang (1991); Kabanemi et al. (1998); Smith, Tortorelli and Tucker (1998)]. With the development of computer hardware, 3-dimensional simulations

---

[1] School of Science, Northwestern Polytechnical University, Xi'an 710129, China, jieouyang@nwpu.edu.cn

[2] National Engineering Research Center for Advanced Polymer Processing Technology, Zhengzhou University, Zhengzhou 450002,China, ctliu@zzu.edu.cn

of mold filling process have been realized by using Navier-Stokes equations and different numerical methods [Hetu et al. (1998); Pichelin and Coupez (1998); Kim and Turng (2006); Zhou, Geng and Li (2005); Chang and Yang (2001); Zhou and Turng (2007)]. The papers mentioned above studied the mold filling process without the consideration of the interface motion. The development of the interface capturing or tracking techniques, such as volume of fluid method (VOF) and the level set method and so on, has propelled greatly the development of mold filling simulation techniques. Many papers studying mold filling process coupled with interface tracking techniques can be found [Khayat, Elsin and Kim (2000); Holm and Langtangen (1999); Luoma and Voller (2000); Soukane and Trochu (2006); Ayad and Rigolot (2002); Geng, Li and Zhou (2006); Kim, Park and Lee (2003); Zhou, Yan and Zhang (2008); Au (2005); Khor et al. (2010)]. In these papers, the viscoelastic properties of materials were ignored. However, the melt for mold filling process is often viscoelastic materials. Some papers made a study on mold filling problems with viscoelastic free surfaces [Bonito, Picasso and Laso (2006); Tomé et al. (2000)]. However, these papers studied the problem with only viscoelastic fluid phase considered and the gas phase in the cavity ignored, in which case complex boundary conditions must be properly dealt with. Yang et al. (2010) proposed a model for mold filling process in which the governing equations for the viscoelastic fluid (melt phase) and the Newtonian fluid (gas phase) are successfully united into a system of generalized Navier-Stokes equations, avoiding dealing with complex boundary conditions.

On the other hand, for fiber reinforced composites mold filling process, fibers motion and orientation must be considered as well as free interface evolution. However, many papers focused more on the mechanical properties of solid fiber reinforced composites than considering the forming process of fiber reinforced composites [Yerramalli and Waas (2004); Verbis, Tsinopoulos and Polyzos (2002); Pyo and Lee (2009); Bohm, Han and Eckschlager (2004)]. Ngo and Tamma (2004) described an in-depth study of the mathematical and computational developments towards the formulation of a fully integrated and comprehensive approach to the modeling of composite manufactured net-shaped parts. Tang and Advani (2005) proposed an optimization method to simulate the motion of long flexible fibers in shear flow. Some papers simulated the fiber orientation in mold filling process [Henry De Frahan et al. (1992); McGrath and Wille (1995); Kim, Park and Jo (2001); Chung and Kwon (2002)].

However, to our knowledge, a dynamic simulation for fiber reinforced composites for mold filling process can not be found. The difficulty lies in that both fibers transformation and orientation and interface evolution must be considered simultaneously. In our previous work [Yang et al. (2010)] that proposed the viscoelastic-

Newtonian model for mold filling process, the interface formed by the viscoelastic melt and the gas in the mold can be captured at each time step. In this paper, a gas-solid-liquid three-phase model, including the information of fluid flow, interface evolution and dynamics of fibers, is proposed based on our viscoelastic-Newtonian model [Yang et al. (2010)]. The description for dynamics of fibers in a Langrangian coordinate are coupled successfully with both the level set method for interface evolution and fluid flow description in Eulerian coordinates. Classical numerical methods, such as finite volume method, can be easily used to solve the model for the direct dynamic numerical simulation of fiber reinforced composites mold filling process. The information about fiber transformation and orientation and interface evolution can be obtained at each time step. The changes of pressure and velocity etc. *versus* time can also be captured.

2 Viscoelastic-Newtonian model for mold filling process [Yang et al. (2010)]

2.1 Level set equation for interface evolution

We use the level set method to describe the interface Γ between the two sub-domains. The level set function φ usually takes the form of a signed distance to the interface, whereby the zero level set $\varphi = 0$ represents the points $\mathbf{x}(\mathbf{x} = (x, y))$ on the actual interface Γ. The interface is evolved by the velocity (u, v). It can be described by the advection equation in the Eulerian coordinate [Osher and Fedkiw (2001)] .

$$\frac{\partial \varphi}{\partial t} + \mathbf{u} \cdot \nabla \varphi = 0 \tag{1}$$

A reinitialization algorithm must be applied to keep φ as the algebraic distance to the interface. We use the corrected algorithm presented by Sussman et al. (1998) to improve the accuracy of solving the reinitialization equation. A local correction item, $\omega \delta_\varepsilon(\varphi)|\nabla \varphi|$, is added to the reinitialization equation. The revised reinitialization equation can be described as

$$\begin{cases} \frac{\partial \varphi}{\partial t_r} + sign(\varphi_0)(|\nabla \varphi| - 1) = \omega \delta_\varepsilon(\varphi)|\nabla \varphi| \\ \varphi(x, y, 0) = \varphi_0(x, y) \end{cases} \tag{2}$$

where ω is the weight coefficient, t_r is a pseudo time, $sign(\varphi_0)$ is the sign function of φ which is defined as

$$sign(\varphi_0) = \frac{\varphi_0}{\sqrt{\varphi_0^2 + [\min(\Delta x, \Delta y)]^2}} \tag{3}$$

Here,Δx and Δy are the grid widths along x and y direction respectively, and $[\min(\Delta x, \Delta y)]^2$ is used to avoid denominator's dividing by zero. $\delta_\varepsilon(\varphi)$ is the Dirac function defined as

$$\delta_\varepsilon(\varphi) = \begin{cases} \frac{1}{2\varepsilon}(1 + \cos(\pi\varphi/\varepsilon)) & |\varphi| < \varepsilon \\ 0 & otherwise \end{cases} \tag{4}$$

Here, ε is a small positive number about a grid width. See Sussman et al. (1998) for more details.

2.2 Governing equations for Viscoelastic-Newtonian flow

In mold filling process, since the gas-phase and the liquid-phase are immiscible and the Mach number of the gas is very small, both the gas-phase and the liquid-phase can be regarded as incompressible flows.

Since the melt for mold filling is viscoelastic, a proper constitutive equation describing the rheology of polymer melts must be chosen. The extended pom-pom (XPP) constitutive equation is based on molecular theory of rheology and can provide a good fitting to the rheology of polymer melts and concentrated solutions [Verbeeten, Peters and Baaijens (2001); Verbeeten, Peters and Baaijens (2002)]. The stresses τ_{xx}, τ_{xy} and τ_{yy} satisfy the following XPP constitutive relation which is described as a tensor form

$$f(\lambda,\tau)\tau + \lambda_{0b}\overset{\nabla}{\tau} + G_0(f(\lambda,\tau) - 1)\mathbf{I} + \frac{\alpha}{G_0}\tau\cdot\tau = 2\lambda_{0b}G_0\mathbf{d} \tag{5}$$

where $f(\lambda,\tau) = 2\frac{\lambda_{0b}}{\lambda_{0s}}e^{\nu(\lambda-1)}\left(1 - \frac{1}{\lambda}\right) + \frac{1}{\lambda^2}\left[1 - \frac{\alpha I_{\tau\cdot\tau}}{3G_0^2}\right]$, $\lambda = \sqrt{1 + \frac{|I_\tau|}{3G_0}}$, $\nu = \frac{2}{q}$. Here λ is the backbone stretch used to represent the stretched degree of the polymer molecule, α is a material parameter defining the amount of anisotropy, λ_{0b} and λ_{0s} denote the orientation and backbone stretch relaxation time-scales of the polymer chains respectively, G_0 is the linear relaxation modulus, $\mathbf{I}$ is the identity tensor, q is the number of arms of polymer chains and $\mathbf{d}$ is the strain tensor. The superscript symbol ∇ over τ represents the upper-convected derivative. The parameter ν was incorporated into the model by Blackwell, Mcleish and Harlen (2000) to remove the discontinuity in the derivative of the extensional viscosity, and presented in the differential approximation of the original pom-pom model.

In Yang et al. (2010), the governing equations for the viscoelastic fluid with an XPP constitutive equation and the Newtonian fluid are successfully united into a system of generalized Navier-Stokes equations by defining the Heaviside function

which is described in dimensionless form as follows.

$$
H_\varepsilon(\varphi) = \begin{cases} 0, & \varphi < -\varepsilon \\ \frac{1}{2}\left[1 + \frac{\varphi}{\varepsilon} + \sin(\pi\varphi/\varepsilon)/\pi\right], & |\varphi| \leq \varepsilon \\ 1, & \varphi > \varepsilon \end{cases} \tag{6}
$$

Then the governing equations for viscoelastic-Newtonian flow can be expressed as follows.

continuity

$$
\frac{\partial \rho}{\partial t} + \frac{\partial u}{\partial x} + \frac{\partial v}{\partial y} = 0 \tag{7}
$$

u-momentum

$$
\frac{\partial(\rho u)}{\partial t} + \frac{\partial(\rho u u)}{\partial x} + \frac{\partial(\rho v u)}{\partial y} - \frac{1}{Re}\left(\frac{\partial^2(\mu u)}{\partial x^2} + \frac{\partial^2(\mu u)}{\partial y^2}\right) = -\frac{\partial p}{\partial x}H_\varepsilon(\varphi)
$$
$$
+ \frac{(\beta-1)}{Re}\left(\frac{\partial^2(\mu u)}{\partial x^2} + \frac{\partial^2(\mu u)}{\partial y^2}\right)H_\varepsilon(\varphi) + \frac{1}{Re}\frac{\partial \tau_{xx}}{\partial x}H_\varepsilon(\varphi) + \frac{1}{Re}\frac{\partial \tau_{xy}}{\partial y}H_\varepsilon(\varphi) \tag{8}
$$

v-momentum

$$
\frac{\partial(\rho v)}{\partial t} + \frac{\partial(\rho u v)}{\partial x} + \frac{\partial(\rho v v)}{\partial y} - \frac{1}{Re}\left(\frac{\partial^2(\mu v)}{\partial x^2} + \frac{\partial^2(\mu v)}{\partial y^2}\right) = -\frac{\partial p}{\partial y}H_\varepsilon(\varphi)
$$
$$
+ \frac{(\beta-1)}{Re}\left(\frac{\partial^2(\mu v)}{\partial x^2} + \frac{\partial^2(\mu v)}{\partial y^2}\right)H_\varepsilon(\varphi) + \frac{1}{Re}\frac{\partial \tau_{yx}}{\partial x}H_\varepsilon(\varphi) + \frac{1}{Re}\frac{\partial \tau_{yy}}{\partial y}H_\varepsilon(\varphi) \tag{9}
$$

where the Reynolds number $Re = \rho_l L U / \mu_l$, $\rho(\varphi) = \xi + (1-\xi)H_\varepsilon(\varphi)$, $\mu(\varphi) = \eta + (1-\eta)H_\varepsilon(\varphi)$, $\xi = \rho_g/\rho_l$, $\eta = \mu_g/\mu_l$, β is the ratio of the Newtonian viscosity and the total viscosity, the subscript l and g denote the liquid phase and the gas phase respectively, L and U are parameters for non-dimensionalization.

constitutive

$$
\varpi\frac{\partial \psi}{\partial t} + \nabla \cdot (\varpi \mathbf{u}\psi) - \nabla \cdot (\Lambda \nabla \psi) = S_\psi \tag{10}
$$

The constants and functions in Eq. (10) are defined in Table 1 [Aboubacar et al. (2005)], where the Weissenberg number is defined as We $= \lambda_{0b}U/L$.

Table 1: Definition of the constants and functions in the constitutive equation

Equation	ϖ	ψ	Λ	S_ψ
τ_{xx} normal stress	We	τ_{xx}	0	$2(1-\beta)\frac{\partial u}{\partial x} + 2\mathrm{We}\tau_{xx}\frac{\partial u}{\partial x} + 2\mathrm{We}\tau_{xy}\frac{\partial u}{\partial y} - f(\lambda,\tau)\tau_{xx} - [f(\lambda,\tau)-1]\frac{1-\beta}{\mathrm{We}} - \alpha\frac{\mathrm{We}}{1-\beta}(\tau_{xx}^2 + \tau_{xy}^2)$
τ_{xy} shear stress	We	τ_{xy}	0	$(1-\beta)\left(\frac{\partial v}{\partial x} + \frac{\partial u}{\partial y}\right) + \mathrm{We}\tau_{xx}\frac{\partial v}{\partial x} + \mathrm{We}\tau_{yy}\frac{\partial u}{\partial y} - f(\lambda,\tau)\tau_{xy} - \alpha\frac{\mathrm{We}}{1-\beta}\tau_{xy}(\tau_{xx} + \tau_{yy})$
τ_{yy} normal stress	We	τ_{yy}	0	$2(1-\beta)\frac{\partial v}{\partial y} + 2\mathrm{We}\tau_{yy}\frac{\partial v}{\partial y} + 2\mathrm{We}\tau_{xy}\frac{\partial v}{\partial x} - f(\lambda,\tau)\tau_{yy} - [f(\lambda,\tau)-1]\frac{1-\beta}{\mathrm{We}} - \alpha\frac{\mathrm{We}}{1-\beta}(\tau_{yy}^2 + \tau_{xy}^2)$
τ_{zz} stress	We	τ_{zz}	0	$-f(\lambda,\tau)\tau_{zz} - [f(\lambda,\tau)-1]\frac{1-\beta}{\mathrm{We}} - \alpha\frac{\mathrm{We}}{1-\beta}\tau_{zz}^2$

3 Modeling for fiber reinforced polymer mold filling process

The idea of particle orbit model [Tsuji, Tanaka and Ishida (1992)] is introduced to our model for fiber reinforced polymer mold filling process, in which the fluid flows are solved in Eulerian coordinate, while the dynamics of fibers are considered in Langrangian coordinate. An additional source term $\mathbf{S}_p = \left((S_p)_x, (S_p)_y \right)^T$ is added to the momentum equations (8) and (9) in order to reflect the effects of fibers on polymer melt. On the other hand, the effects of melt on fibers are described by the resultant force $\mathbf{F}$ imposed on fibers. The two aspects will be discussed below in detail.

3.1 Dynamics of fibers

Dynamics of fibers include translation and orientation processes caused by the resultant force $\mathbf{F}$ imposed on fibers by fluid.

3.1.1 Translation

The translation of fiber i is described by Newton's law of motion, which is expressed as follows.

$$\mathbf{F}_i = m_i \mathbf{a}_i \tag{11a}$$

or

$$\mathbf{F}_i = m_i \frac{d\mathbf{u}_i}{dt} \tag{11b}$$

where, $\mathbf{F}_i = \left((F_x)_i, (F_y)_i \right)$ is the resultant force imposed on fiber i, m_i is the mass of fiber i, $\mathbf{a}_i = \left((a_x)_i, (a_y)_i \right)$ is the acceleration of fiber i, and $\mathbf{u}_i = (u_i, v_i)$ is the velocity of fiber i. The velocity $\mathbf{u}_i$ at time $n+1$ can be got if $\mathbf{F}_i$ is known according to the following finite difference approximation.

$$\mathbf{u}_i^{n+1} = \mathbf{u}_i^n + \frac{\mathbf{F}_i \Delta t}{m_i} \tag{12}$$

where $\mathbf{u}_i^n$ is the velocity of fiber i at time n, Δt is the time step.

Several different forces may be imposed on each fiber. In this paper, we consider two major forces imposed on fibers, that is, the drag force and pressure gradient force.

The drag force can be expressed as Tran-Cong, Gay and Efstathios (2004).

$$(\mathbf{F}_d)_i = (C_d)_i (A_p)_i \rho_l |\mathbf{u}_l - \mathbf{u}_i| (\mathbf{u}_l - \mathbf{u}_i)/2 \tag{13}$$

where $(C_d)_i$ is the coefficient of the drag force for fiber i, $(A_p)_i$ is the projected surface area of the fiber normal to the direction of its motion, $\mathbf{u}_l$ is the polymer melt velocity. The choice of C_d is very important for the computation of drag force. The formula presented by Tran-Cong, Gay and Efstathios (2004) is adopted in this paper, that is

$$C_d = \frac{24}{Re_f}\frac{d_A}{d_n}\left(1 + \frac{0.15}{\sqrt{c}}\left(\frac{d_A}{d_n}Re_f\right)^{0.687}\right) + \frac{0.42\left(\frac{d_A}{d_n}\right)^2}{\sqrt{c}\left(1 + 4.25\times 10^4\left(\frac{d_A}{d_n}Re_f\right)^{-1.16}\right)}$$

(14)

where Re_f is the Reynolds number of fiber, $d_A = \sqrt{4A_p/\pi}$ is the surface equivalent sphere diameter, $d_n = \sqrt[3]{6V_f/\pi}$ is the volume equivalent sphere diameter or nominal diameter, V_f is the fiber volume, and c is the fiber circularity. The relationship between fiber circularity c and fiber aspect ratio r_c is $c = 2.62r_c^{2/3}/(1+2r_c)$. The Reynolds number of fiber i $(Re_f)_i$ can be computed as follows.

$$(Re_f)_i = \frac{\rho_l\,|\mathbf{u}_{vir} - \mathbf{u}_i|\,(d_n)_i}{\mu_l}$$

(15)

Here, $\mathbf{u}_{vir}$ is the virtual velocity at the centroid of fiber i. $\mathbf{u}_{vir}$ can be computed by bilinear interpolation with the schematic diagram shown in Fig. 1 [Ouyang and Li (1999)]. (x_i,y_j), (x_{i+1},y_j), (x_i,y_{j+1}) and (x_{i+1},y_{j+1}) are four corner points of a control volume, the melt velocities on which are $\mathbf{u}_{i,j}$, $\mathbf{u}_{i+1,j}$, $\mathbf{u}_{i,j+1}$ and $\mathbf{u}_{i+1,j+1}$, respectively. Suppose the center of mass of fiber i locates at $(x_i + \delta x, y_j + \delta y)$. Then the virtual velocity at the centroid of fiber i can be computed as follows.

$$\mathbf{u}_{vir} = \frac{b_{i,j}\mathbf{u}_{i,j} + b_{i+1,j}\mathbf{u}_{i+1,j} + b_{i,j+1}\mathbf{u}_{i,j+1} + b_{i+1,j+1}\mathbf{u}_{i+1,j+1}}{dxdy}$$

(16)

where

$$b_{i,j} = (dx - \delta x)(dy - \delta y)$$

(17)

$$b_{i+1,j} = \delta x(dy - \delta y)$$

(18)

$$b_{i,j+1} = (dx - \delta x)\delta y$$

(19)

$$b_{i+1,j+1} = \delta x\delta y$$

(20)
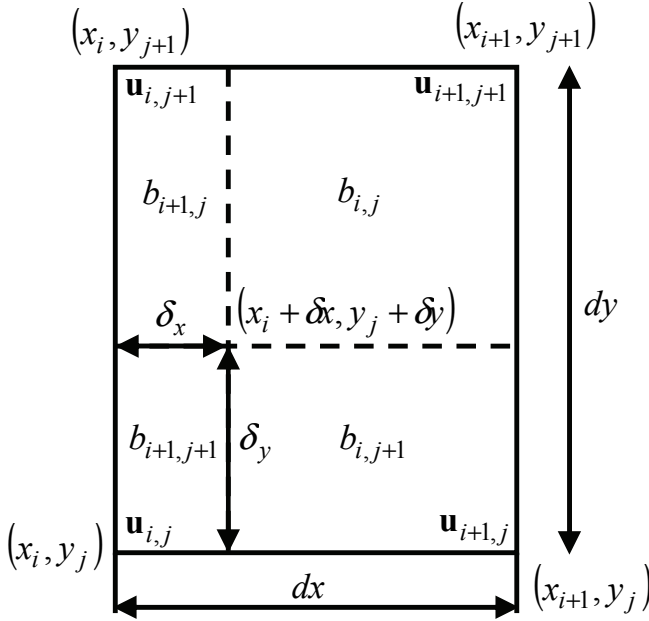
Figure 1: Schematic diagram of bilinear interpolation

The pressure gradient force can be expressed as $(V_f)_i \nabla p_i$. Enclosing the drag force and the pressure gradient force, the resultant force $\mathbf{F}_i$ imposed on fiber i can be expressed as

$$\mathbf{F}_i = (\mathbf{F}_d)_i + (V_f)_i \nabla p_i \tag{21}$$

Thus, the velocity $\mathbf{u}_i^{n+1}$ can be computed according to Eq. (12).

The new position of fiber i at time $n+1$ can be expressed as follows.

$$\mathbf{W}_i^{n+1} = \mathbf{W}_i^n + \mathbf{u}_i^{n+1} \Delta t \tag{22}$$

where $\mathbf{W}_i = (W_x, W_y)$ is the position vector of fiber i.

3.1.2 Orientation

The orientation of a fiber can be expressed in three dimensional space coordinates as shown in Fig. 2. Since the fiber has a circular cross-section and does not bend, the orientation is determined by ϕ and θ. ϕ is the angle between x-axis and the projection of the fiber on xy-plane. θ is the angle between the fiber vector and z-axis.
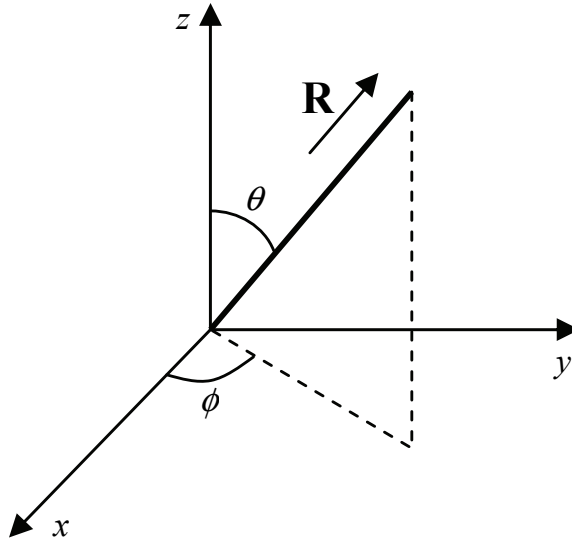
Figure 2: A fiber orientation vector in Cartesian coordinates.

Jeffery's equation [Jeffery (1922)] describes the orientation of a fiber as

$$\dot{\mathbf{R}} = \boldsymbol{\omega} \cdot \mathbf{R} + \lambda_f \left(\boldsymbol{\varepsilon} \cdot \mathbf{R} - \boldsymbol{\varepsilon} : \mathbf{RRR} \right) \tag{23}$$

where, $\mathbf{R}$ is the unit vector aligned with the fiber axis, $\boldsymbol{\omega} = \left(\nabla \mathbf{u}^T - \nabla \mathbf{u} \right)/2$, $\boldsymbol{\varepsilon} = \left(\nabla \mathbf{u}^T + \nabla \mathbf{u} \right)/2$ is the deformation rate tensor, $\lambda_f = \left(r_c^2 - 1 \right)/\left(r_c^2 + 1 \right)$. A dot over a variable denotes the time derivative throughout the paper. Zhou and Lin (2008) derive the fiber orientation distribution from the classic mechanics and kinetic theory. They depict fiber orientation for a planar flow field aligned with the $x - y$ plane. For convenience, denote $\partial u/\partial y = \dot{\gamma}$, $\partial v/\partial x = k\dot{\gamma}$, $\partial u/\partial x = j\dot{\gamma}$ and $\partial v/\partial y = -j\dot{\gamma}$. Then the variance ratio of ϕ and θ can be expressed as follows according to Jeffery's equation [Zhou and Lin (2008)].

$$\dot{\phi} = \frac{1}{2} \left[\lambda_f (k+1) \cos(2\phi) + k - 1 - 2\lambda \sin(2\phi) \right] \dot{\gamma} \tag{24}$$

$$\dot{\theta} = \frac{1}{4} \lambda_f \sin(2\theta) \left[2j \cos(2\phi) + (k+1) \sin(2\phi) \right] \dot{\gamma} \tag{25}$$

3.2 *Effect of fibers on polymer flow*

An additional source term $\mathbf{S}_p = \left((S_p)_x, (S_p)_y \right)^T$ is added to the momentum equations (8) and (9) in order to reflect the effects of fibers on fluid.

u-momentum

$$
\frac{\partial (\rho u)}{\partial t} + \frac{\partial (\rho u u)}{\partial x} + \frac{\partial (\rho v u)}{\partial y} - \frac{1}{Re} \left(\frac{\partial^2 (\mu u)}{\partial x^2} + \frac{\partial^2 (\mu u)}{\partial y^2} \right) =
$$

$$
-\frac{\partial p}{\partial x} H_\varepsilon (\varphi) + \frac{(\beta - 1)}{Re} \left(\frac{\partial^2 (\mu u)}{\partial x^2} + \frac{\partial^2 (\mu u)}{\partial y^2} \right) H_\varepsilon (\varphi) + \frac{1}{Re} \frac{\partial \tau_{xx}}{\partial x} H_\varepsilon (\varphi)
$$

$$
+ \frac{1}{Re} \frac{\partial \tau_{xy}}{\partial y} H_\varepsilon (\varphi) - (S_p)_x H_\varepsilon (\varphi) \quad (26)
$$

v-momentum

$$
\frac{\partial (\rho v)}{\partial t} + \frac{\partial (\rho u v)}{\partial x} + \frac{\partial (\rho v v)}{\partial y} - \frac{1}{Re} \left(\frac{\partial^2 (\mu v)}{\partial x^2} + \frac{\partial^2 (\mu v)}{\partial y^2} \right) =
$$

$$
-\frac{\partial p}{\partial y} H_\varepsilon (\varphi) + \frac{(\beta - 1)}{Re} \left(\frac{\partial^2 (\mu v)}{\partial x^2} + \frac{\partial^2 (\mu v)}{\partial y^2} \right) H_\varepsilon (\varphi) + \frac{1}{Re} \frac{\partial \tau_{yx}}{\partial x} H_\varepsilon (\varphi)
$$

$$
+ \frac{1}{Re} \frac{\partial \tau_{yy}}{\partial y} H_\varepsilon (\varphi) - (S_p)_y H_\varepsilon (\varphi) \quad (27)
$$

The computation of $\mathbf{S}_p$ will be discussed in Section 6.1.

4 Numerical methods

4.1 Numerical methods for level set and the reinitialization equation

Level set evolution equation (1) and the reinitialization equation (2) are solved by the finite difference method on a rectangular grid. The spatial derivatives are discretized by the 5th-order Weighted Essentially Non-Oscillatory (WENO) scheme [Jiang and Peng (2000); Osher and Shu (1991)] and the temporal derivatives are discretized by the 3rd-order Total Variation Diminishing Runge-Kutta (TVD-R-K) scheme [Shu and Osher (1989)].

4.2 Numerical methods for governing equations of the viscoelastic-Newtonian flow

The finite volume SIMPLE methods on a non-staggered grid are used to solve the governing equations (7), (26), (27) and (10). A non-staggered grid arrangement, which stores all the variables at the same physical location and employs only one set of control volumes, is shown in Fig. 3, where the dashed lines are the faces of control volumes or cells and the intersection points of the solid lines are the nodes on which all the physical quantities are located [Tao (2001)].
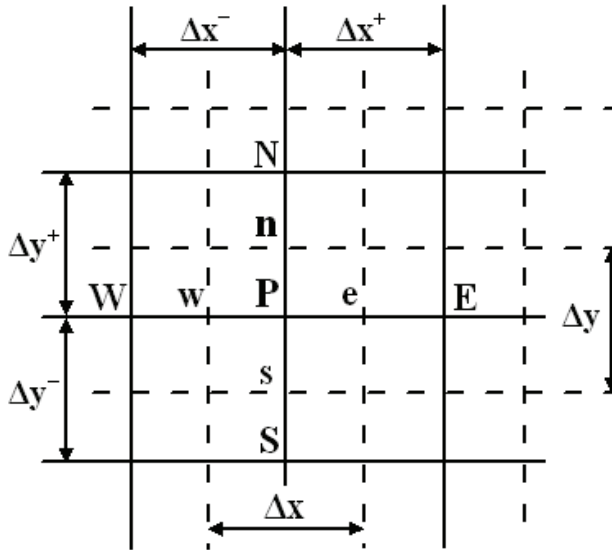
Figure 3: Sketch map of the non-staggered meshes

4.2.1 Continuity equation

The continuity equation (7) can be discretized to be the following form by integrating in the control volume

$$((\rho u)_e - (\rho u)_w)\,\Delta y + ((\rho v)_n - (\rho v)_s)\,\Delta x = 0 \tag{28}$$

4.2.2 Momentum equations

The discretization of the momentum equations (26) and (27) can be written as the following form by a generalized quantity ψ, that is,

$$a_P\psi_P = a_E\,\psi_E + a_W\,\psi_W + a_N\,\psi_N + a_S\,\psi_S + S_\psi \tag{29}$$

where S_ψ is the source term in the momentum equation. The coefficients a_E, a_W, a_N, a_S, a_P can be expressed as the combination of the convection term and the diffusion term, i.e.,

$$a_E = D_e A(|P_e|) + \max(-F_e, 0) \quad a_W = D_w A(|P_w|) + \max(F_w, 0)$$

$$a_N = D_n A(|P_n|) + \max(-F_n, 0) \quad a_S = D_s A(|P_s|) + \max(F_s, 0) \tag{30}$$

$$a_P = a_E + a_W + a_N + a_S + \Delta x \Delta y \rho / \Delta t$$

where P_e, P_s, P_w, P_n are the Peclet numbers on the cell faces, F_e, F_s, F_w, F_n are the cell faces flux, and D_e, D_s, D_w, D_n denote diffuse derivatives on cell faces. The form of $A\left(|P_\Delta|\right)$ can be different under different discretization schemes for the convection term. For example, $A\left(|P_\Delta|\right)$ equals to 1 for the upwind scheme while $1 - 0.5\,|P_\Delta|$ for a central scheme. We take $A\left(|P_\Delta|\right) = 1$ in this paper. All the coefficients are formulated as follows.

$$F_e = (\rho u)_e \Delta y \quad D_e = \frac{\mu_e \Delta y}{(x_E - x_P)\,Re} \quad P_e = \frac{F_e}{D_e}$$

$$F_w = (\rho u)_w \Delta y \quad D_w = \frac{\mu_w \Delta y}{(x_P - x_W)\,Re} \quad P_w = \frac{F_w}{D_w} \tag{31}$$

$$F_n = (\rho v)_n \Delta x \quad D_n = \frac{\mu_n \Delta x}{(y_N - y_P)\,Re} \quad P_n = \frac{F_n}{D_n}$$

$$F_s = (\rho v)_s \Delta x \quad D_s = \frac{\mu_s \Delta x}{(y_P - y_S)\,Re} \quad P_s = \frac{F_s}{D_s}$$

4.2.3 Constitutive equations

The discretization of the constitutive equation (10) can also be written as the following form by a generalized quantity ψ, that is,

$$a_P^\tau \psi_P = a_E^\tau \psi_E + a_W^\tau \psi_W + a_N^\tau \psi_N + a_S^\tau \psi_S + S_\psi^\tau \tag{32}$$

where S_ψ^τ is the source term in the constitutive equation and the coefficients a_E^τ, a_W^τ, a_N^τ, a_S^τ, a_P^τ can be expressed as

$$a_E^\tau = \text{We}\max(-F_e, 0) \quad a_W^\tau = \text{We}\max(F_w, 0)$$

$$a_N^\tau = \text{We}\max(-F_n, 0) \quad a_S^\tau = \text{We}\max(F_s, 0) \tag{33}$$

$$a_P^\tau = a_E^\tau + a_W^\tau + a_N^\tau + a_S^\tau + \text{We}\Delta x \Delta y / \Delta t$$

Here the expressions of F_e, F_s, F_w, F_n are identical to (31).

The discrete constitutive equation (32) can be solved only in the liquid part. However, the free surface stress conditions have to be dealt with as has been done in Tomé et al. (2008) and Tomé et al. (2002). In our previous work, we have tried to avoid doing this by defining another Weissenberg number $\text{We}' = \text{We} \times H_\varepsilon(\varphi)$ and let $S_\psi' = S_\psi^\tau \times H_\varepsilon(\varphi)$. Eqs. (32) and (33) then change into

$$a_P^\tau \psi_P = a_E^\tau \psi_E + a_W^\tau \psi_W + a_N^\tau \psi_N + a_S^\tau \psi_S + S_\psi' \tag{34}$$

$$a_E^\tau = \text{We}' \max(-F_e, 0) \quad a_W^\tau = \text{We}' \max(F_w, 0)$$

$$a_N^\tau = \text{We}' \max(-F_n, 0) \quad a_S^\tau = \text{We}' \max(F_s, 0) \tag{35}$$

$$a_P^\tau = a_E^\tau + a_W^\tau + a_N^\tau + a_S^\tau + \text{We}' \Delta x \Delta y / \Delta t + \varepsilon_1$$

where ε_1 is a small positive number for avoiding dividing by zero. Thus the constitutive equation can be regarded to be hold in the whole computational domain. In particular, as for the gas phase in the cavity, Eq. (34) will be $\varepsilon_1 \psi_P = 0$, which implies $\psi_P = 0$. By doing this, we see that the stresses τ_{xx}, τ_{xy} and τ_{yy} will appear only in the melt phase, although the constitutive equations are solved in the whole computational domain.

4.2.4 *Formulation of the cell-face stresses*

Since non-staggered grid approach is adopted, a special velocity interpolation scheme, originally designed by Rhie and Chow (1983), is required. According to Rhie and Chow's special interpolation method, the cell face velocity u_f is calculated by linear interpolation of the momentum equations, with exception of the pressure gradient which is evaluated as in the staggered approach [Darwish, Whiteman and Bevis (1992)].

In the momentum equation, it is necessary to compute the stresses at cell faces from stress values at cell centers and there is a stress-velocity coupling problem, akin to the pressure-velocity coupling, that needs to be properly solved [Oliveira, Pinho and Pinto (1998)]. If a linear interpolation of cell centered values of stress is used to compute face values, a possible lack of connectivity between the stress and velocity fields may result [Oliveira, Pinho and Pinto (1998)]. Oliveira, Pinho and Pinto (1998) developed a new interpolation technique for UCM constitutive equation inspired on that of Rhie and Chow (1983). Here, the interpolation technique in Oliveira, Pinho and Pinto (1998) is extended to XPP constitutive equation.

When a stress component τ_{xy} is required at a cell face e, in the momentum equation, it is obtained by arithmetic averaging the stress equations written for cell P and for its neighbor E across face e, with the exception that velocity differences straddling the face are to be evaluated directly [Oliveira, Pinho and Pinto (1998)]. Thus, the spirit of Rhie and Chow (1983) interpolation for the face velocity is followed, guarantying a good connection between a face stress and the velocity values at either side of the face [Oliveira, Pinho and Pinto (1998)]. This procedure is equivalent to

defining the cell-face stress as follows [Yang et al. (2010)].

$$
(\tau_{xy})_e = \overline{(\tau_{xy})_P + (\tau_{xy})_E}
$$
$$
+ \left(\frac{\Delta}{a'^\tau_P}\right)_e \left[We\overline{\tau}^0_{xy}\left(\frac{u_E - u_P}{x_E - x_P}\right)^0 + ((1-\beta) + We\overline{\tau}^0_{xx})\left(\frac{v_E - v_P}{x_E - x_P}\right)^0 \right]_e
$$
$$
\overline{\left[\frac{\Delta}{a'^\tau_P}We\tau^0_{xy}\left(\frac{\partial u}{\partial x}\right)^0\right]_P + \left[\frac{\Delta}{a'^\tau_P}We\tau^0_{xy}\left(\frac{\partial u}{\partial x}\right)^0\right]_E}
$$
$$
\overline{-\left[\frac{\Delta}{a'^\tau_P}((1-\beta) + We\tau^0_{xx})\left(\frac{\partial v}{\partial x}\right)^0\right]_P + \left[\frac{\Delta}{a'^\tau_P}((1-\beta) + We\tau^0_{xx})\left(\frac{\partial v}{\partial x}\right)^0\right]_E}
$$

$$(36)$$

where $\overline{\tau}^0_{xy} = \overline{(\tau^0_{xy})_P + (\tau^0_{xy})_E}$, $\overline{\tau}^0_{xx} = \overline{(\tau^0_{xx})_P + (\tau^0_{xx})_E}$. The sup script 0 in $S'_{\tau_{xy}}$ denotes the values at previous time step and $\Delta = \Delta x \Delta y$ is the area of the control volume. Define $a'^\tau_P = a^\tau_P / \alpha_\tau$, where α_τ is the relaxation factor. The long bar denotes the linear interpolation formula, that is, $\overline{Q_P + Q_E} = (1 - f^x_P)Q_P + f^x_P Q_E$, where f^x_P is the interpolation factor expressed as

$$
f^x_P = \frac{x_e - x_P}{x_E - x_P} \tag{37}
$$

Analogously to Eq. (36), we have

$$
(\tau_{xx})_e = \overline{(\tau_{xx})_P + (\tau_{xx})_E} + \left(\frac{\Delta}{a'^\tau_P}\right)_e (2(1-\beta) + 2We\overline{\tau}^0_{xx})\left(\frac{u_E - u_P}{x_E - x_P}\right)^0
$$
$$
\overline{-\left[\frac{\Delta}{a'^\tau_P}(2(1-\beta) + 2We\tau^0_{xx})\left(\frac{\partial u}{\partial x}\right)^0\right]_P + \left[\frac{\Delta}{a'^\tau_P}(2(1-\beta) + 2We\tau^0_{xx})\left(\frac{\partial u}{\partial x}\right)^0\right]_E}
$$

$$(38)$$

where $\overline{\tau}^0_{xx} = \overline{(\tau^0_{xx})_P + (\tau^0_{xx})_E}$

$$
(\tau_{xy})_n = \overline{(\tau_{xy})_P + (\tau_{xy})_N}
$$
$$
+ \left(\frac{\Delta}{a'^\tau_P}\right)_n \left[We\overline{\tau}^0_{xy}\left(\frac{v_N - u_P}{y_N - y_P}\right)^0 + ((1-\beta) + We\overline{\tau}^0_{yy})\left(\frac{u_N - u_P}{y_N - y_P}\right)^0 \right]
$$
$$
\overline{-\left[\frac{\Delta}{a'^\tau_P}We\tau^0_{xy}\left(\frac{\partial v}{\partial y}\right)^0\right]_P + \left[\frac{\Delta}{a'^\tau_P}We\tau^0_{xy}\left(\frac{\partial v}{\partial y}\right)^0\right]_N}
$$
$$
\overline{-\left[\frac{\Delta}{a'^\tau_P}((1-\beta) + We\tau^0_{yy})\left(\frac{\partial u}{\partial y}\right)^0\right]_P + \left[\frac{\Delta}{a'^\tau_P}((1-\beta) + We\tau^0_{yy})\left(\frac{\partial u}{\partial y}\right)^0\right]_N}
$$

$$\tag{39}$$

where $\overline{\tau}_{xy}^0 = \overline{(\tau_{xy}^0)_P + (\tau_{xy}^0)_N}$, $\overline{\tau}_{yy}^0 = \overline{(\tau_{yy}^0)_P + (\tau_{yy}^0)_N}$.

$$(\tau_{yy})_n = \overline{(\tau_{yy})_P + (\tau_{yy})_N} + \left(\frac{\Delta}{a'^\tau_P}\right)_n (2(1-\beta) + 2We\overline{\tau}_{yy}^0)\left(\frac{v_N - v_P}{y_N - y_P}\right)^0$$

$$\overline{-\left[\frac{\Delta}{a'^\tau_P}(2(1-\beta) + 2\lambda\tau_{yy}^0)\left(\frac{\partial v}{\partial y}\right)^0\right]_P + \left[\frac{\Delta}{a'^\tau_P}(2(1-\beta) + 2\lambda\tau_{yy}^0)\left(\frac{\partial v}{\partial y}\right)^0\right]_N}$$

$$\tag{40}$$

where $\overline{\tau}_{yy}^0 = \overline{(\tau_{yy}^0)_P + (\tau_{yy}^0)_N}$.

5   Numerical test for a broken dam problem

We take the broken dam problem shown in Fig. 4 [Yue, Lin and Patel (2003)] to test the validity of the methodology. The computational domain is 5a×1.25a, where a is the width of the water body. *s* and *h* denote the surge front position and the remaining height of the water column respectively and are used to measure the spreading velocity and the falling rate of the water column. See Yue, Lin and Patel (2003) for more details about the parameters setting. A uniform grid of 200×50 is used. Fig. 5(a) shows changes of the surge fronts along *x*-direction *versus* time together with those in Yue, Lin and Patel (2003). Fig. 5(b) shows the changes of the remaining water column height *versus* time together with those in Yue, Lin and Patel (2003). Fig. 6 gives the positions of the interface at some select times. All the results are in accordance with those in [Yue, Lin and Patel (2003)], which shows the validity of our methodology.
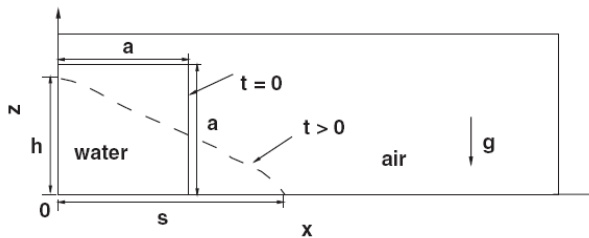
Figure 4: Schematic for two-dimensional broken dam
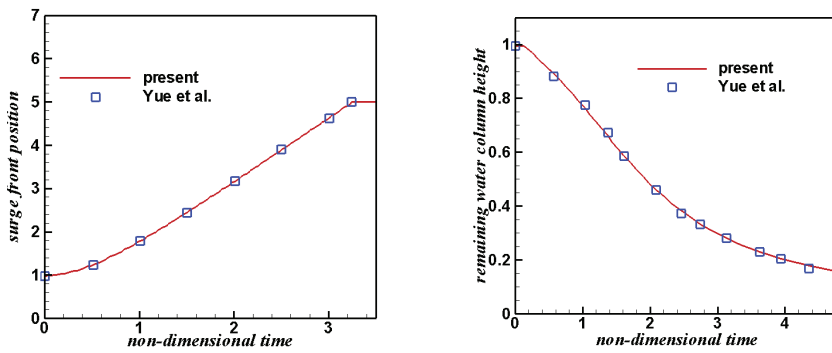
(a) Surge front position s along x-direction versus time.   (b) Remaining water column height *h versus* time.

Figure 5: Two-dimensional broken dam
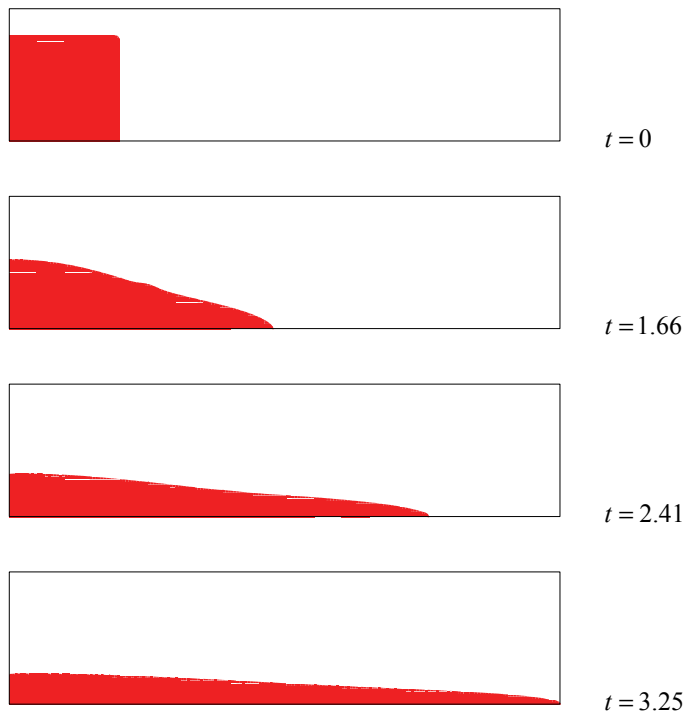
Figure 6: Free surface position at selected times the shadow areas represent the water

6   Results for mold filling and analysis

6.1   Computational domain and parameters setting

Sketch map and the computational area of the injection mold are shown in Fig. 7(a), in which the shaded area, i.e. the vertical middle plane of the mold, is the computational domain (Fig. 7(b)). The initial interface is set to be a semicircle with a radius 0.5 which is shown in Fig. 7(b) with shaded area.

(a)   Sketch map and the computational area (dark area) of the mold

(b)   Computational domain and initial interface
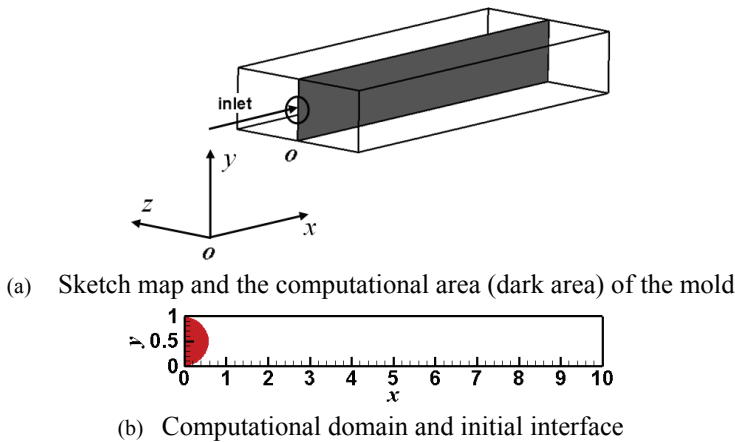
Figure 7: Mold and computational domain

All the parameters appeared in this section are in dimensionless forms. Suppose the length and width of the computational area are 10.0 and 1.0 respectively. We use a 200×20 grid for computation.

Short glass fibers are used for the simulation. The density of the fibers is $2.49 \times 10^3 kg/m^{-3}$. The initial fibers, including the positions, angles ϕ and θ, are generated randomly. Every fiber is regarded as a short rigid rod with a slenderness ratio 40. 200 fibers are distributed randomly in the initial melt (within the semicircular interface) which is shown in Fig. 8 with a partial enlargement of the image within the square box being illustrated on the right column. In the mold filling process, new fibers will enter the cavity at each time step, so new fibers must be generated randomly near the inlet at every time step. A total number of 6000 fibers are generated during the mold filling process and the volume fraction of the fibers will be 37.5%. For the flow field computation, we set $Re = 0.01$ and $We = 0.01$. The inlet velocity is set to be $u = 20.0 \times (y - 0.5)^2 + 5.0, y \in [0, 1]$.

The momentum exchange source $\mathbf{S}_p$ in a control volume (width Δx and height Δy)
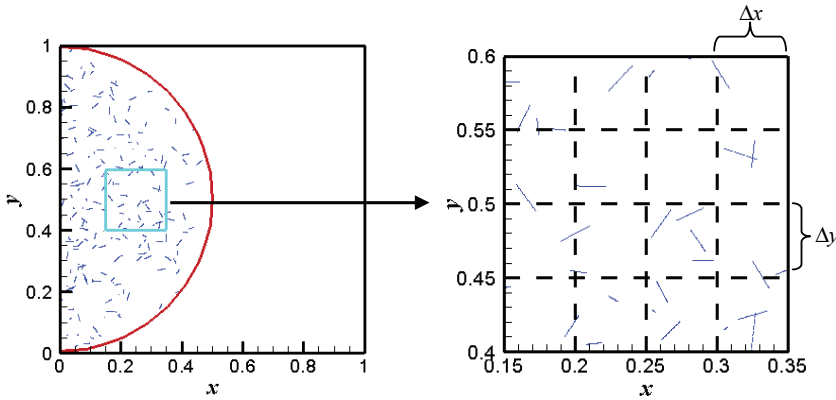
Figure 8: Initial interface and initial generated fibers

is calculated as

$$\mathbf{S}_p = \frac{1}{V_{cell}} \sum_{i=1}^{N^*} \mathbf{F}_i$$

Here, N^* is the number of fibers in this control volume, $\mathbf{F}_i$ is the resultant force imposed on fiber i in this control volume and $V_{cell} = \Delta x \Delta y$ is the area of the control volume.

6.2 Interface evolution

Fig. 9 shows the interface evolution *versus* time in the molding process. Just as pointed by Han (2007), the melt spreads in an approximately radial manner at first and then fills the corners, followed by forward movement to fill the rest of the empty mold cavity. In doing so, the melt front changes from a circular shape to an almost flat profile. At $t = 6.4$, the mold is completely filled with melt without any voids.
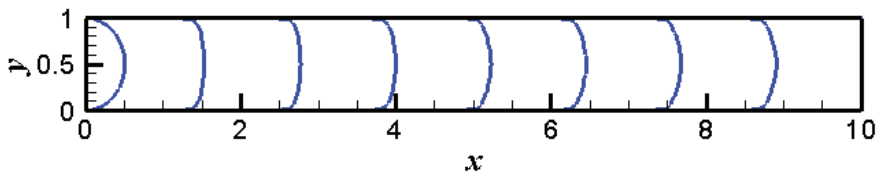
Figure 9: Interface evolution at time t=0, 0.8, 1.6, 2.4, 3.2, 4.0, 4.8, 5.6

6.3   Fountain flow

Fig. 10 shows the velocity distributions at three different positions $x = 2.5$, $x = 5.0$ and $x = 7.5$. The velocity profiles are parabolic with almost the same values at different positions.

Fig. 11 gives the velocity vectors in the melt phase at dimensionless time $t = 3.2$. The fountain flow is obviously observed, that is, polymer material has approached the flow front from the center and has been diverted towards the wall.
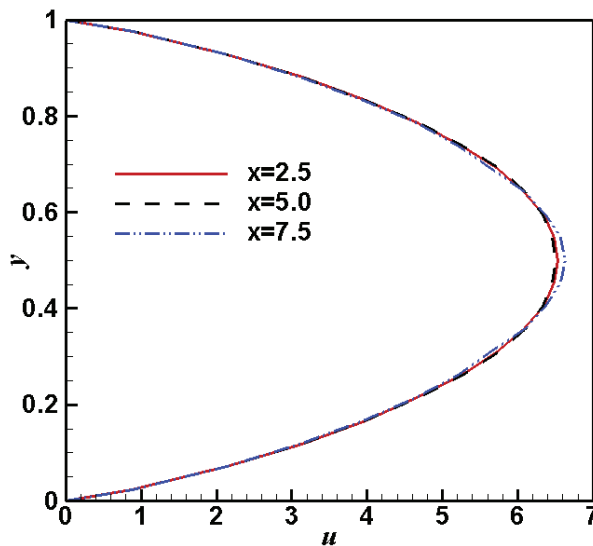
Figure 10: Velocity distributions at $x = 2.5$, $x = 5.0$ and $x = 7.5$

6.4   Pressure distribution

The pressure contours at different time are presented in Fig. 12, from which we see that the pressure values are degressive from the inlet to the end of the cavity and the inlet always keeps the maximum pressure value. The pressure in the mold keeps increasing until the mold is filled with melt.

6.5   Dynamics of fibers

A dynamics of fibers at different time during mold filling process is shown in Fig. 13. The skin-core-skin structure of fibers can be seen in Fig. 13. In the skin region, the fibers have higher tendency to align along the melt flow direction, while in the core region, the fibers are randomly oriented. The reason is that strong shearing
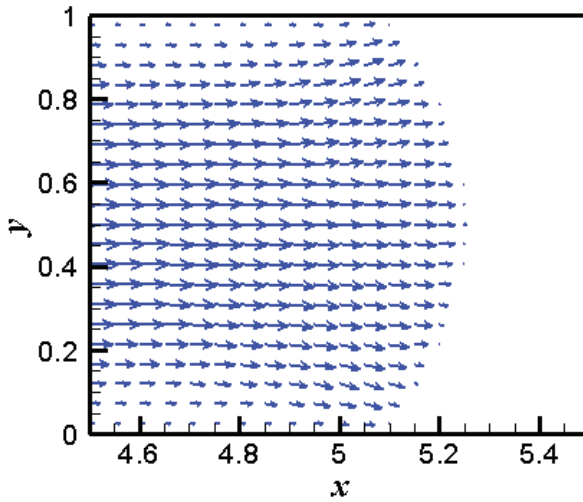
Figure 11: Velocity vectors in the melt phase at dimensionless time $t = 3.2$
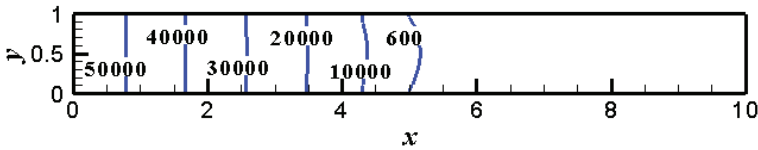
(a) $t = 3.2$
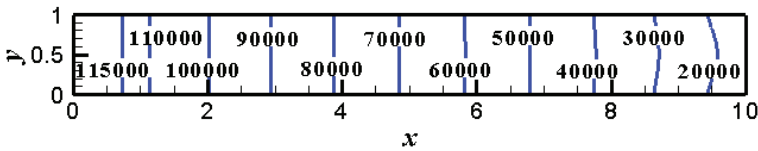
(b) $t = 6.4$

Figure 12: Pressure distribution at different time

takes place near the upper and lower side walls of the mold while the shear rate near the horizontal mid-line of the mold is low. Fig. 14 shows the comparison between our numerical result in an local enlarged image (left) with that of the experiment (right) made by Fung and Li (2006), from which we see the accordance of our numerical result with that of the experiment. Moreover, from Fig. 14 we can see

the fibers concentration in skin layers is greater than that in core layer.

When we change the slenderness ratio of fibers to 10, the skin-core-skin can still be seen as shown in Figs. 15-16.

In order to see the trajectory of fiber motion more clearly, five fibers with initial positions $(0.317, 0.534)$, $(0.326, 0.414)$, $(0.271, 0.606)$, $(0.326, 0.827)$ and $(0.271, 0.301)$ are tracked. The trajectories of the centroids of three fibers are shown in Fig. 17. Fibers that lie near $y = 0.5$ move almost straight forward, because the v-velocity is almost zero. Fibers that lie on the upper and lower sides of $y = 0.5$ move gradually toward the upper and lower sides of the mold, the reason is obviously that the existence of the fountain flow in the mold filling process.

6.6   *Perturbation effect of fibers on fluid flows*

Fig. 18 shows the comparison of the maximum values of u-velocity between the numerical results without fibers in the melt and those with fibers in the melt. It can be seen that the velocity curve *versus* time with fibers is oscillatory while that without fibers is smooth. The reason clearly lies in the perturbation effect of fibers on fluid flows.

6.7   *Convergence*

Two meshes are used for computations, which are shown in Table 2. The time step Δt is determined by restrictions due to CFL condition and viscosity [Sussman et al. (1998)].

$$\Delta t_c = \min_{\Omega} \left(\frac{\Delta x}{|u|} \right)$$

$$\Delta t_\mu = \min_{\Omega} \left(\frac{3}{14} \frac{\rho Re \Delta x^2}{\mu} \right)$$

The eventual restriction on the time step is then

$$\Delta t^{n+1} = \frac{1}{2} \min \left(\Delta t_c, \Delta t_\mu \right)$$

The u velocities under different meshes are shown in Fig. 19, which show the convergence of the meshes.

7   Conclusion

In this paper, a gas-solid-liquid three-phase model is proposed and a direct dynamic numerical simulation for fiber reinforced composites mold filling process is made.
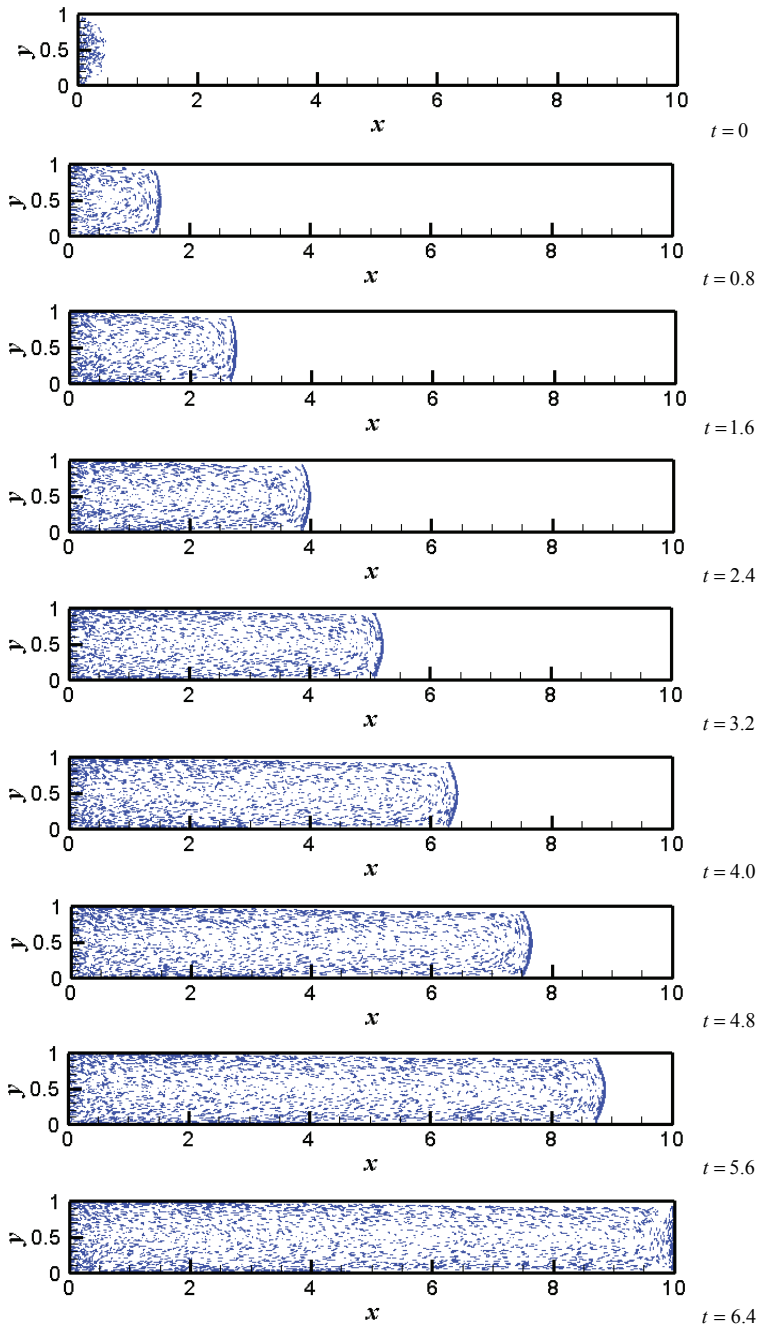
Figure 13: Translation and orientation of fibers *versus* time during mold filling process with a slenderness ratio of 40
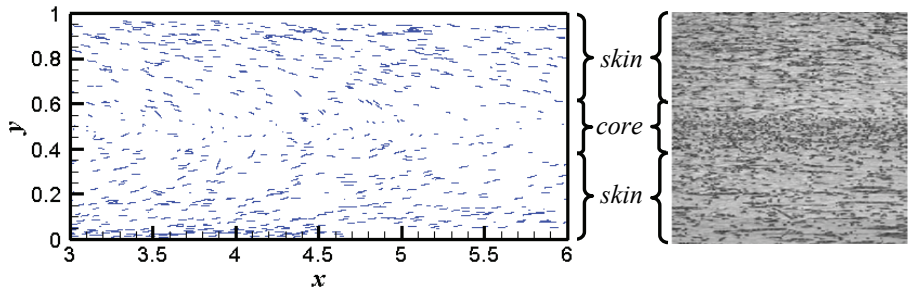
Figure 14: Comparison of skin-core-skin structure of fibers between the results of numerical methods and that of experiment at $t=6.4$

Table 2: Definition of the constants and functions in the constitutive equation

Meshes	Volumes	Degrees of freedom $\mathbf{u}, P, \tau, \varphi)$	$\Delta x\,(\Delta y)$
Coarse	200×20	52000	0.05
Fine	400×40	208000	0.025

The particle orbit model for dynamics of fibers in a Langrangian coordinate are coupled successfully with both the level set method for interface evolution and fluid flow description in Eulerian coordinates. The positions of the interface and the transformation and orientation of fibers at each time step are captured. The melt front changes from a circular shape to an almost flat profile during the mold filling process. The skin-core-skin structure of fibers during the mold filling process is found which is in accordance with experimental results. The slenderness ratio of fibers does not change the skin-core-skin structure of fibers. The velocity profiles are parabolic with almost the same values at different positions and a fountain flow is found in the simulation. The pressure in the mold keeps increasing until the mold is filled with melt and the maximum value of pressure is always achieved at the inlet. A perturbation effect of fibers on fluid flow can be found in the simulation. The model is easy to be solved by classical numerical methods and convenient to apply on other fields of chemical engineering.
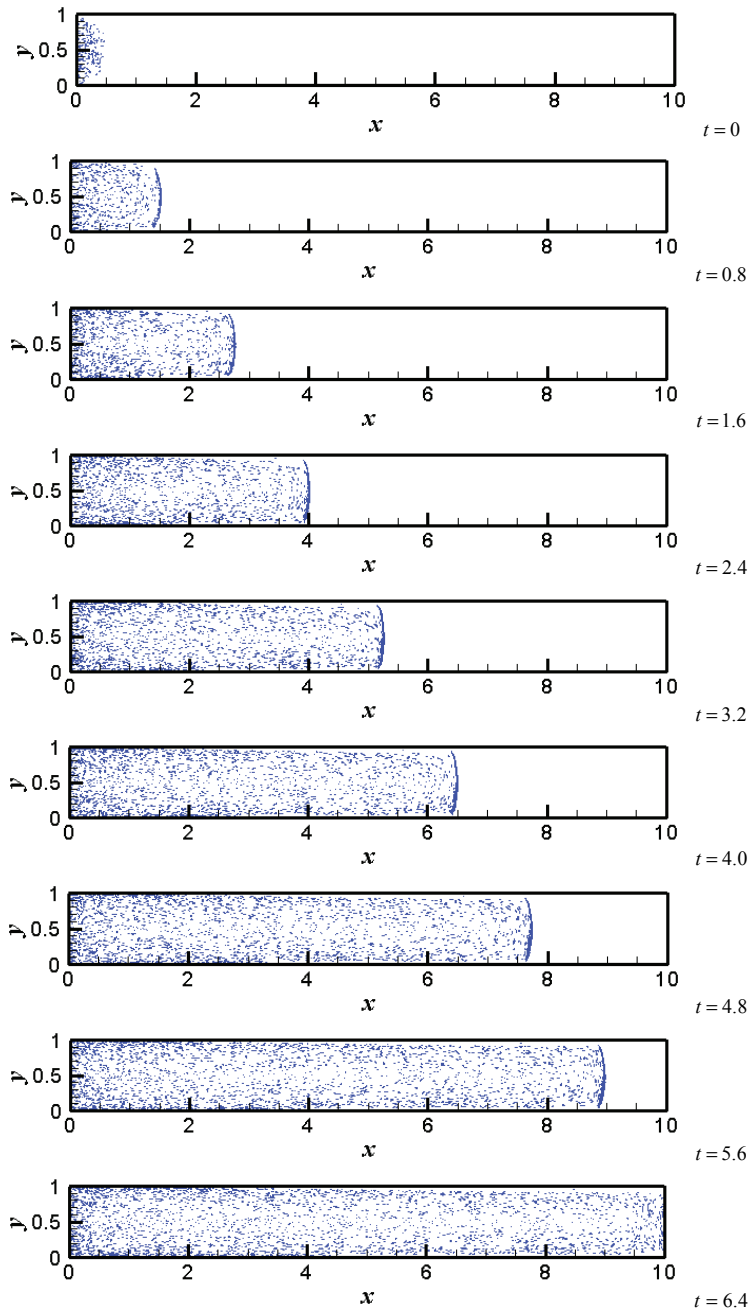
Figure 15: Translation and orientation of fibers *versus* time during mold filling process with a slenderness ratio of 10
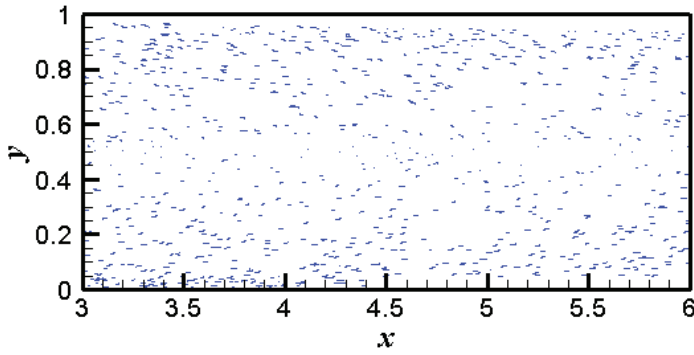
Figure 16: Skin-core-skin structure of fibers at slenderness ratio 10 at *t*=6.4
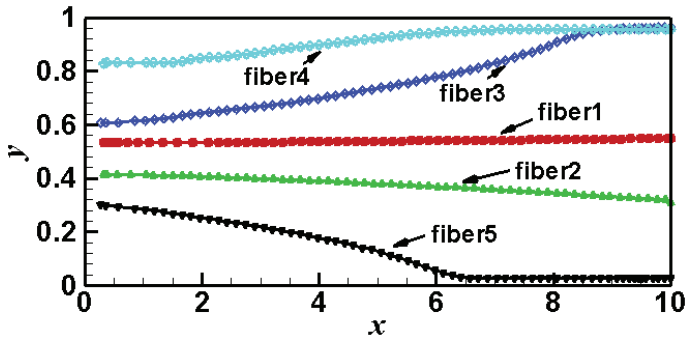
Figure 17: The trajectories of the centroids of five fibers (Initial position: fiber 1(0.317, 0.534), fiber 2(0.326, 0.414), fiber 3(0.271, 0.606), fiber 4(0.326, 0.827) and fiber 5(0.271, 0.301))
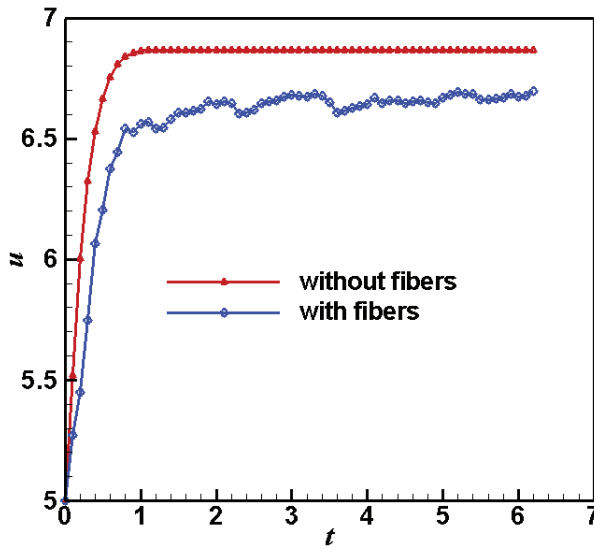
Figure 18: Comparison of the maximum values of *u*-velocity with fibers and those without fibers *versus* time
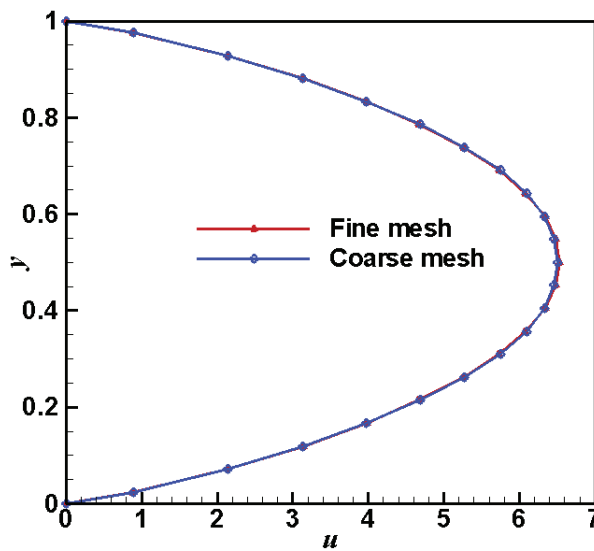
Figure 19: Mold filling: *u* velocity at $x = 2.5$ under different meshes

References

Aboubacar, M.; Aguayo, J.P.; Phillips, P.M.; Phillips, T.N., Tamaddon-Jahromi, H.R.; Snigerev, B.A.; Webster, M.F. (2005): Modelling pom-pom type models with high-order finite volume schemes. *Journal of Non-Newtonian Fluid Mechanics*, vol. 126, no. 2-3, pp. 207-220.

Au, C.K. (2005): A geometric approach for injection mould filling simulation. *International Journal of Machine Tools & Manufacture*, vol. 45, no. 1, pp. 115-124.

Ayad, R.; Rigolot, A. (2002): The VOF-G/FEV model for tracking a polymer-air interface in the injection moulding process. *Journal of Mechanical Design*, vol. 124, no. 4, pp. 813-821.

Blackwell, R.J.; Mcleish, T.C.B.; Harlen, O.G. (2000): Molecular drag-strain coupling in branched polymer melts. *Journal of Rheology*, vol. 44, no. 1, pp. 121-136.

Bohm, H.J.; Han, W.; Eckschlager, A. (2004): Multi-inclusion unit cell studies of reinforcement stresses and particle failure in discontinuously reinforced ductile matrix composites. *CMES: Computer Modeling in Engineering & Sciences*, vol. 5, no. 1, pp. 5-20.

Bonito, A.; Picasso, M.; Laso, M. (2006): Numerical simulation of 3D viscoelastic flows with free surfaces. *Journal of Computational Physics*, vol. 215, no. 2, pp. 691-716.

Chang, R.Y.; Yang, W. H. (2001): Numerical simulation of mold filling in injection molding using a three-dimensional finite volume approach. *International Journal for Numerical Methods in Fluids*, vol. 27, no. 2, pp. 125-148.

Chiang, H.H.; Hieber, C.A.; Wang, K.K. (1991): A unified simulation of the filling and postfilling stages in injection-molding. 1: Formulation. *Polymer Engineering and Science*, vol. 31, no. 2, pp. 116-124.

Chung, D.H.; Kwon, T.H. (2002): Fiber orientation in the processing of polymer composites. *Korea-Australia Theology Journal*, vol. 14, no. 4, pp. 175-188.

Darwish, M.S.; Whiteman, J.R.; Bevis, M.J. (1992): Numerical modeling of viscoelastic liquids using a finite-volume method. *Journal of Non-Newtonian Fluid Mechanics*, vol. 45, pp. 311-337.

Fung, K.L.; Li, R.K.Y. (2006): Mechanical properties of short glass fibre reinforced and functionalized rubber-toughened PET blends. *Polymer Testing*, vol. 25, no. 7, pp. 923-931.

Geng, T.; Li, D.Q.; Zhou, H.M. (2006): Three-dimensional finite element method for the filling simulation of injection molding. *Engineering with Computers*, vol.

21, no. 4, pp. 289-295.

Han, C.D. (2007): *Rheology and Processing of Polymeric Materials*. Oxford University Press.

Henry De Frahan, H.; Verleye, V.; Dupret, F.; Crochet, M.J. (1992): Numerical prediction of fiber orientation in injection molding. *Polymer Engineering and Science*, vol. 32, no. 4, pp. 254-266.

Hetu, J.F.; Gao, D.M.; Garcia-Rejon, A.; Salloum G. (1998): 3D finite element method for the simulation of the filling stage in injection molding. *Polymer Engineering and Science*, vol. 38, no. 2, pp. 223-236.

Holm, E.J.; Langtangen, H.P. (1999): A unified finite element model for the injection molding process. *Computer Methods in Applied Mechanics and Engineering*, vol. 178, no. 3-4, pp. 413-429.

Jeffery, G.B. (1922): The motion of ellipsoidal particles immersed in a viscous fluid. *Proceedings of the Royal Society of London*, *Series A*, vol. 102, pp. 161-179.

Jiang, G.S.; Peng, D.P. (2000): Weighted ENO schemes for Hamilton-Jacobi equations. *Siam Journal on Scientific Computing*, vol. 21, no. 6, pp. 2126-2143.

Kabanemi, K.K.; Vaillancourt, H.; Wang, H.; Salloum, G. (1998): Residual stresses, shrinkage, and warpage of complex injection molded products: numerical simulation and experimental validation. *Polymer Engineering and Science*, vol. 38, no. 1, pp. 21-37.

Khayat, R.E.; Elsin, W.; Kim, K. (2000): An adaptive boundary element approach to transient free surface flow as applied to injection molding. *International Journal for Numerical Methods in Fluids*, vol. 33, no. 6, pp. 847-868.

Khor, C.Y.; Ariff, Z.M.; Che Ani, F.; Abdul Mujeebu, M.; Abdullah, M.K.; Abdullah, M.Z.; Joseph, M.A. (2010): Three-dimensional numerical and experimental investigations on polymer rheology in meso-scale injection molding. *International Communications in Heat and Mass Transfer*, vol. 37, no. 2, pp. 131-139.

Kim, E.G.; Park, J.K.; Jo, S.H. (2001): A study on fiber orientation during the injection molding of fiber-reinforced polymeric composites. *Journal of Materials Processing Technology*, vol. 111, no. 1-3, pp. 225-232.

Kim, M.S.; Park, J.S.; Lee, W.I. (2003): A new VOF-based numerical scheme for the simulation of fluid flow with free surface. Part II: application to the cavity filling and sloshing problems. *International Journal for Numerical Methods in Fluids*, vol. 42, no. 7, pp. 791-812.

Kim, S.W.; Turng, L.S. (2006): Three-dimensional numerical simulation of injection molding filling of optical lens and multiscale geometry using finite element method. *Polymer Engineering and Science*, vol. 46, no. 9, pp. 1263-1274.

Luoma, J.A.; Voller, V.R. (2000): An explicit scheme for tracking the filling front during polymer mold filling. *Applied Mathematical Modeling*, vol. 24, no. 8-9, pp. 575-590.

McGrath, J.J.; Wille, J.M. (1995): Determination of 3D fiber orientation distribution in thermoplastic injection molding. *Composites Science and Technology*, vol. 53, no. 2, pp. 133-143.

Ngo, N.D.; Tamma, K.K. (2004): An integrated comprehensive approach to the modeling of resin transfer molded composite manufactured net-shaped parts. *CMES: Computer Modeling in Engineering & Sciences*, vol.5, no.2, pp. 103-133.

Oliveira, P.J.; Pinho, F.T.; Pinto, G.A. (1998): Numerical simulation of non-linear elastic flows with a general collocated finite-volume method, *Journal of Non-Newtonian Fluid Mechanics*, vol. 79, pp. 1-43.

Osher, S.; Fedkiw, R.P. (2001): Level set methods: An overview and some recent results. *Journal of Computational Physics*, vol.169, no .2, pp. 463-502.

Osher, S.; Shu, C.W., (1991): High-order essentially non-oscillatory schemes for Hamilton- Jacobi equations. *SIAM Journal on Numerical Analysis*, vol. 28, pp. 907-922.

Ouyang, J.; Li, J.H. (1999): Particle-motion-resolved discrete model for simulating gas-solid fluidization. *Chemical Engineering Science,* vol.54, no.13, pp. 2077-2083.

Pichelin, E.; Coupez, T. (1998): Finite element solution of the 3D mold filling problem for viscous incompressible fluid. *Computer Methods in Applied Mechanics and Engineering*, vol. 163, no. 1-4, pp. 359-371.

Pyo, S.H.; Lee, H.K. (2009): Micromechanical analysis of aligned and randomly oriented whisker-/short fiber-reinforced composites. *CMES: Computer Modeling in Engineering & Sciences*, vol. 40, no. 3, pp. 271-305.

Rhie, C.M.; Chow, W.L. (1983): Numerical study of the turbulent flow past an airfoil with trailing edge separation. *AIAA Journal*, vol. 21, pp. 1525-1532.

Shu, C.W.; Osher, S. (1989): Efficient implementation of essentially non-oscillatory shock-capturing schemes, II. *Journal of Computational Physics*, vol. 83, pp. 32-78.

Smith, D.E.; Tortorelli, D.A.; Tucker, C.L. (1998): Analysis and sensitivity analysis for polymer injection and compression molding. *Computer Methods in Applied Mechanics and Engineering*, vol. 167, no. 3-4, pp. 325-344.

Soukane, S.; Trochu, F. (2006): Application of the level set method to the simulation of resin transfer molding. *Composites Science and Technology*, vol. 66, no. 7-8, pp. 1067-1080.

Sussman, M.; Fatemi, E.; Smereka, P.; Osher, S. (1998): An improved level

set method of incompressible two-phase ?ows, *Computers and Fluid,* Vol. 27, pp. 663-680.

Tang, W.Z.; Advani, S.G. (2005): Dynamic simulation of long flexible fibers in shear flow. *CMES: Computer Modeling in Engineering & Sciences*, vol. 8, no.2, pp. 165-176.

Tao, W.Q. (2001): *Numerical Heat Transfer*. Xi'an Jiaotong University Press.

Tomé, M.F.; Castelo, A.; Ferreira, V.G.; Mckee, S. (2008): A finite difference technique for solving the Oldroyd-B model for 3D-unsteady free surface flows. *Journal of Non-Newtonian Fluid Mechanics*, vol. 154, no. 2-3, pp. 179-206.

Tomé, M.F.; Castelo, A.; Murakami, J.; Cuminato, J.A.; Minghim, R.; Oliveira, M.C.F., Mangiavacchi, N.; Mckee, S. (2000): Numerical simulation of axisymmetric free surface flows. *Journal of Computational Physics*, vol. 157, no. 2, pp. 441-472.

Tomé, M.F.; Mangiavacchi, N.; Cuminato, J.A.; Castelo, A.; Mckee, S. (2002): A finite difference technique for simulating unsteady viscoelastic free surface flows. *Journal of Non-Newtonian Fluid Mechanics*, vol. 106, no. 2-3, pp. 61-106.

Tran-Cong, S.; Gay, M.; Efstathios, E. (2004): Drag coefficients of irregularly shaped particles. *Powder Technology*, vol. 139, no. 1, pp. 21-32.

Tsuji, Y.; Tananka, T.; Ishida, T. (1992): Lagrangian numerical simulation of plug flow of cohesionless particles in a horizontal pipe. *Powder Technology*, vol. 71, no.3, pp. 239-250.

Verbeeten, W.M.H.; Peters, G.W.M.; Baaijens, F.P.T. (2001): Differential constitutive equations for polymer melts: The extended Pom-Pom model. *Journal of Rheology*, vol. 45, no. 6, pp. 823-844.

Verbeeten, W.M.H.; Peters, G.W.M.; Baaijens, F.P.T. (2002): Viscoelastic analysis of complex polymer melt flows using the eXtended Pom-Pom model. *Journal of Non-Newtonian Fluid Mechanics*, vol. 108, no. 1-3, pp. 301-326.

Verbis, J.T.; Tsinopoulos, S.V.; Polyzos, D. (2002): Elastic wave propagation in fiber reinforced composite materials with non-uniform distribution of fibers. *CMES: Computer Modeling in Engineering & Sciences*, vol. 3, no. 6, pp. 803-814.

Wang, V.W.; Hieber, C.A.; Wang, K.K. (1986): Dynamic simulation and graphics for the injection-molding of 3-dimensional thin parts. *Journal of Polymer Engineering*, vol. 7, no.1, pp. 21-45.

Yang, B.X.; Ouyang, J.; Li, Q.; Zhao, Z.F.; Liu, C.T. (2010): Modeling and simulation of the viscoelastic fluid mold filling process by level set method. *Journal of Non-Newtonian Fluid Mechanics*, doi:10.1016/j.jnnfm.2010.06.011.

Yerramalli, C.S.; Waas, A.M. (2004): The effect of fiber diameter on the compressive strength of composites - A 3D finite element based study. *CMES: Computer Modeling in Engineering & Sciences*, vol. 6, no.1, pp. 1-16.

Yue, W.S.; Lin, C.L.; Patel, V.C. (2003): Numerical simulation of unsteady multidimensional free surface motions by level set method. *International Journal for Numerical Methods in Fluids*, vol. 42, no. 8, pp. 853-884.

Zhou, H.M.; Geng, T.; Li, D.Q. (2005): Numerical filling simulation of injection molding based on 3D finite element model. *Journal of Reinforced Plastics and Composites*, vol. 24, no. 8, pp. 823-830.

Zhou, K.; Lin, J.Z. (2008): Three dimensional fiber orientation distribution in two dimensional flows. *Fibers and Polymers*, vol. 9, no. 1, pp. 39-47.

Zhou, J.; Turng, L.S. (2007): Three-dimensional numerical simulation of injection mold filling with a finite-volume method and parallel computing. *Advances in Polymer Technology*, vol. 25, no. 4, pp. 247-258.

Zhou, H.M.; Yan, B.; Zhang, Y. (2008): 3D filling simulation of injection molding based on the PG method. *Journal of Materials Processing Technology*, vol. 204, no. 1-3, pp. 475-480.